Full-Wave Analysis of a Wide Class of Microstrip Resonators Fabricated on Magnetized Ferrites With Arbitrarily Oriented Bias Magnetic Field

Germán León, Rafael R. Boix, *Member, IEEE,* and Francisco Medina, *Senior Member, IEEE*

***Abstract*—A numerical code has been developed for the full-wave determination of the resonant frequencies and quality factors of microstrip patches with right-angle corners of arbitrary shape in the case in which the substrate of the patches is a magnetized ferrite with arbitrarily oriented bias magnetic field. The code is based on the solution of an electric-field integral equation by means of Galerkin's method in the spectral domain. The evaluation of the infinite integrals arising from the application of the numerical method is efficiently carried out by means of a technique based on the interpolation of the spectral dyadic Green's function. The numerical results obtained indicate that microstrip patches fabricated on ferrite substrates present cutoff frequency regions in which resonances cannot occur owing to the excitation of magnetostatic modes. The limits of these cutoff regions are shown to be dependent on the orientation and the magnitude of the bias magnetic field, on the shape of the patches, and even on the nature of every particular resonant mode. The numerical results also show that the resonant frequencies of microstrip patches on magnetized ferrites can always be tuned over a wide frequency range provided the orientation of the bias magnetic field is suitably chosen.**

***Index Terms*—Magnetic tuning, magnetostatic modes, microstrip resonators, microwave ferrites, spectral-domain approach.**

I. Introduction

RESONANT microstrip patches can be used either as antennas or as components of oscillators and filters in microwave integrated circuits. Although the most conventional microstrip patches are the rectangular and circular patches, other geometries such as the rectangular ring [1], the H-shaped patch [1], and the meander-shaped patch [2] have proven to be useful because of their size reduction capabilities (e.g., in the design of antenna arrays, antennas for personal communication systems, ...). This means that the algorithms developed for the analysis of resonant microstrip patches should cover a spectrum of geometries as wide as possible. Apart from their shape, the nature of the substrate of microstrip patches is another interesting degree of freedom for the designer of circuits and antennas. Although the most commonly used substrate materials are dielectrics, magnetized ferrites have proven to have potential application as substrates of microstrip patches. For instance, several researchers have reported that resonant microstrip patches printed on ferrite substrates can be used in the fabrication of tunable band rejection filters [3] and tunable bandpass filters [4], [5]. Also, measurements have shown that the operating resonant frequency of microstrip antennas printed on ferrite substrates can be varied over a wide frequency range by adjusting the bias magnetic field [6]. Apart from that, ferrite substrates can be used for reducing the radar cross section of microstrip antennas under certain conditions [7]–[9] and for achieving linearly, as well as circularly polarized microstrip antennas with a single feed [10]–[12]. Finally, it should be pointed out that when ferrite materials are used as substrates of microstrip phased arrays, wide-angle impedance matching can be obtained by dynamically adjusting the bias magnetic field with scan angle [11], [13].

In this paper, the authors present an algorithm for the determination of the resonant frequencies and quality factors of microstrip patches with right-angle corners of arbitrary shape in the case in which the patches are fabricated on magnetized ferrites with arbitrarily oriented bias magnetic field. This algorithm is based on an efficient application of the spectral-domain approach (SDA) [14], [15]. The study carried out in this paper is an ambitious generalization of that published in previous papers [3], [16], [17] where the SDA was applied to the full-wave analysis of microstrip resonators of both circular shape [3], [17] and rectangular shape [16] fabricated on normally biased ferrite substrates. There is also an additional related paper in which rectangular microstrip resonators on in-plane biased ferrite substrates were analyzed by means of the cavity model [18]. However, the drawback of the cavity model is that it fails to explain how the resonances of microstrip patches on ferrite substrates are affected by the excitation of magnetostatic modes along the substrate [17]. Fortunately, the SDA is capable of accounting for the excitation of magnetostatic modes since the information of these modes is included in the spectral dyadic Green's function (in fact, the propagation constants of the magnetostatic modes are complex poles of the aforementioned spectral Green's function [9], [17]).

Concerning the contents of this paper, Section II briefly describes the application of the SDA to the full-wave analysis of microstrip resonators fabricated on ferrite substrates. In this section, a powerful technique is explained, which makes possible the fast computation of infinite integrals arising from the application of the SDA. In Section III, numerical results are presented for the resonant frequencies and quality factors of microstrip patches of different shapes (rectangular, H-, and

Manuscript received January 23, 2001. This work was supported by the Comisión Interministerial de Ciencia y Tecnología, Spain, under Project TIC98-0630.

The authors are with the Microwave Group, Department of Electronics and Electromagnetism, School of Physics, University of Seville, 41012 Seville, Spain (e-mail: boix@cica.es).

Publisher Item Identifier S 0018-9480(02)05206-7.

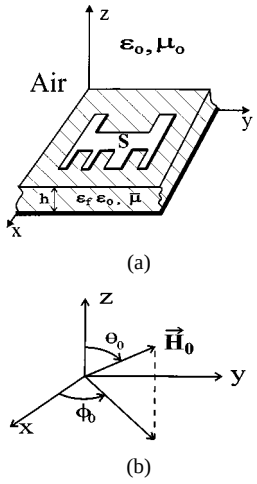

Fig. 1. (a) Microstrip patch with right-angle corners of arbitrary shape on a ferrite substrate. (b) Orientation of the internal bias magnetic field of the ferrite substrate with respect to the coordinate axes shown in (a).

meander shaped) printed on ferrite substrates. Special emphasis is put on showing that the propagation of magnetostatic modes along the ferrite substrates prevents the patches from resonating in certain cutoff frequency bands, and that these cutoff frequency bands vary as a function of the magnitude and the orientation of the bias magnetic field.

II. Formulation of the Problem and Numerical Procedure

Fig. 1(a) shows a microstrip patch with right-angle corners of arbitrary shape printed on a ferrite layer of permittivity $\epsilon_f \epsilon_0$ and thickness h. Both the metallic patch and ground plane are assumed to be perfect electric conductors (PECs) of negligible thickness, and both the ferrite layer and the ground plane are assumed to be of infinite extent along the x and y coordinates. It is also assumed that the electromagnetic fields existing in the patch region show a time dependence of the type $e^{j\omega t}$ (where ω is complex to account for radiation losses), which will be suppressed throughout. Fig. 1(b) shows the orientation of the dc-bias magnetic field existing inside the ferrite layer of Fig. 1(a) with respect to the coordinate axes defined in that figure. In general, the permeability tensor of this ferrite layer can be written as

$$\bar{\mu} = \mu_0 \begin{pmatrix} \mu_{xx} & \mu_{xy} & \mu_{xz} \\ \mu_{yx} & \mu_{yy} & \mu_{yz} \\ \mu_{zx} & \mu_{zy} & \mu_{zz} \end{pmatrix} \tag{1}$$

where the elements of the permeability tensor $\bar{\mu}$ can be obtained in terms of the gyromagnetic ratio $\gamma = 1.759 \cdot 10^{11}$ C/kg, the saturation magnetization of the ferrite layer M_s, the magnitude of the internal bias magnetic field H_0, the linewidth of the ferrite layer ΔH, and the angles ϕ_0 and θ_0 of Fig. 1(b), as shown in [19, eqs. (1)–(4)] and in [20, eqs. (10.37)–(10.40)].

Let S be the metallic surface occupied by the patch of Fig. 1(a), let $\mathbf{j}(x,y)$ be the surface current density existing on the patch under resonant conditions, and let $\bar{\mathbf{G}}_t(x-x', y-y', z \,|\, z')$ be a 2×2 matrix, which stands for the transverse (to z) dyadic Green's function [21] of the conductor-backed ferrite substrate. The transverse electric field $\mathbf{E}_t(x,y,z) = E_x(x,y,z)\hat{\boldsymbol{x}} + E_y(x,y,z)\hat{\boldsymbol{y}}$ created by the current on the patch can be written in terms of $\mathbf{j}(x,y)$ as

$$\mathbf{E}_t(x,y,z) = \int_{S'} \bar{\mathbf{G}}_t\big(x-x', y-y', z \,|\, z'=h\big) \cdot \mathbf{j}\big(x',y'\big)\, dx'\, dy'. \tag{2}$$

If we force that the transverse electric field on the patch surface is zero, the following electric-field integral equation (EFIE) for $\mathbf{j}(x,y)$ is obtained:

$$\int_{S'} \bar{\mathbf{G}}_t\big(x-x', y-y', z=h \,|\, z'=h\big) \cdot \mathbf{j}\big(x',y'\big)\, dx'\, dy' = \mathbf{0}, \qquad (x,y) \in S. \tag{3}$$

In order to solve the EFIE shown above, in this paper, the unknown vector function $\mathbf{j}(x,y)$ has been approximated as a linear combination of known basis functions $\mathbf{j}_j(x,y)$ $(j = 1, \ldots, N)$

$$\mathbf{j}(x,y) = \sum_{j=1}^{N} a_j \mathbf{j}_j(x,y) \tag{4}$$

where $\mathbf{j}_j(x,y)(j = 1, \ldots, N)$ have been chosen to be subsectional rooftop basis functions [22]. With a view to obtaining the unknown coefficients a_j $(j = 1, \ldots, N)$, (4) has been introduced in (3) and the Galerkin's version of the method of moments has been applied to the resulting expression. The final product of these operations turns out to be a homogeneous system of linear equations for a_j $(j = 1, \ldots, N)$ given by

$$\sum_{j=1}^{N} \Gamma_{ij}(\omega) a_j = 0, \qquad i = 1, \ldots, N \tag{5}$$

where

$$\Gamma_{ij}(\omega) = \int_S \big(\mathbf{j}_i^*(x,y)\big)^T \left[\int_{S'} \bar{\mathbf{G}}_t\big(x-x', y-y', z=h \,|\, z'=h; \omega\big) \cdot \mathbf{j}_j(x',y')\, dx'\, dy' \right] dx\, dy, \quad i,j = 1, \ldots, N. \tag{6}$$

Note that the dependence of Γ_{ij} and $\bar{\mathbf{G}}_t$ on the angular frequency ω has been explicitly shown in (5) and (6). The homogeneous system of (5) for the coefficients a_j $(j = 1, \ldots, N)$ only has nontrivial solutions when

$$\det\big[\Gamma_{ij}(\omega)\big] = 0. \tag{7}$$

Equation (7) is an eigenequation for ω, from which the resonant frequencies and quality factors of the resonant modes of the microstrip patch of Fig. 1(a) can be obtained. In fact, let $\omega_m = 2\pi(f_r^m + j f_i^m)$ be the mth complex root of $\det[\Gamma_{ij}(\omega)]$. In that case, the quantity f_r^m stands for the resonant frequency of the mth resonant mode of the patch and the quantity $Q_m = f_r^m / 2 f_i^m$ stands for the quality factor of that resonant mode [14], [15]. The roots of $\det[\Gamma_{ij}(\omega)]$ in the complex ω-plane have been obtained in this paper by means of Muller's method.

Although (2)–(7) seem to provide a straightforward way to the determination of the resonant frequencies and quality factors

of the microstrip patch of Fig. 1(a), the calculation of the quantities $\Gamma_{ij}(i,j=1,\ldots,N)$ via (6) poses problems because the numerical computation of the transverse dyadic Green's function $\bar{\mathbf{G}}_t(x-x',y-y',z=h\,|\,z'=h;\omega)$ for every pair of values of $x-x'$ and $y-y'$ is a task that requires very high CPU times. In order to overcome this inconvenient, the authors of this paper have computed $\Gamma_{ij}(i,j=1,\ldots,N)$ via an alternative expression in the Fourier transform domain since the determination of $\bar{\mathbf{G}}_t$ in that domain can be carried out in a fast, accurate, and stable way for the conductor-backed ferrite substrate of Fig. 1(a) by using the ideas described in [21]. The alternative expression for the computation of Γ_{ij} in the Fourier transform domain is obtained by applying Parseval's theorem to (6) and is given by

$$\Gamma_{ij}(\omega)=\frac{1}{4\pi^2}\int_{-\infty}^{+\infty}\int_{-\infty}^{+\infty}\left(\tilde{\mathbf{j}}_i^*(k_x,k_y)\right)^T\cdot\tilde{\bar{\mathbf{G}}}_t\left(k_x,k_y,z=h\,|\,z'=h;\omega\right)\cdot\tilde{\mathbf{j}}_j(k_x,k_y)\,dk_x\,dk_y,\quad i,j=1,\ldots,N \tag{8}$$

where $\tilde{\mathbf{j}}_j(k_x,k_y)\,(j=1,\ldots,N)$ stand for the two-dimensional Fourier transforms (2D-FTs) of $\mathbf{j}_j(x,y)(j=1,\ldots,N)$ with respect to x and y, and $\tilde{\bar{\mathbf{G}}}_t(k_x,k_y,z=h\,|\,z'=h;\omega)$ stands for the 2D-FT of $\bar{\mathbf{G}}_t(x,y,z=h\,|\,z'=h;\omega)$ (see [21, eq. (11)]).

As explained above, the computational expense required for the determination of $\Gamma_{ij}(i,j=1,\ldots,N)$ via (8) turns out to be much smaller than that required when (6) is used. In spite of this fact, the CPU time involved in the brute-force numerical computation of $\Gamma_{ij}(i,j=1,\ldots,N)$ via (8) is still too high because the integrands of the double infinite integrals show an oscillatory slowly decaying behavior as the spectral variables k_x and k_y grow. In order to save CPU time, the authors of this paper have applied a technique for accelerating the numerical computation of the aforementioned double integrals. The first step of this technique is to express (8) in terms of polar spectral variables k_ρ and k_ϕ ($k_x=k_\rho\cos k_\phi$ and $k_y=k_\rho\sin k_\phi$) as follows:

$$\Gamma_{ij}=\frac{1}{4\pi^2}\int_0^{2\pi}\int_{0(C)}^{+\infty}\left[\left(\tilde{\mathbf{j}}_i^*(k_\rho,k_\phi)\right)^T\cdot\tilde{\bar{\mathbf{G}}}_t\left(k_\rho,k_\phi,z=h\,|\,z'=h;\omega\right)\cdot\tilde{\mathbf{j}}_j\left(k_\rho,k_\phi\right)\right]k_\rho\,dk_\rho\,dk_\phi,\quad i,j=1,\ldots,N \tag{9}$$

where for every value of k_ϕ, C is an integration path in the complex k_ρ-plane located above the complex poles and the complex branch point of $\tilde{\bar{\mathbf{G}}}_t(k_\rho,k_\phi,z=h\,|\,z'=h;\omega)$ (see [23, Fig. 2]). The transformation from (8) to (9) is very advantageous because it makes it possible to reduce from two to one the number of infinite integrals involved in the numerical computation of each quantity Γ_{ij} [24]. The second step of the technique for the fast computation of the integrals of (8) is based on the interpolation of the asymptotic behavior of the spectral dyadic Green's function $\tilde{\bar{\mathbf{G}}}_t(k_\rho,k_\phi,z=h\,|\,z'=h;\omega)$ for large k_ρ in terms of Chebyshev polynomials of the variable $1/k_\rho$ [21]. In fact, it has been found that for practical values of k_ϕ and ω, $\tilde{\bar{\mathbf{G}}}_t(k_\rho,k_\phi,z=h\,|\,z'=h;\omega)$ can be approximately expressed in the interval $k_\rho^{\mathrm{th}}=7/h<k_\rho<\infty$ by means of the interpolating expression

$$\begin{aligned}\tilde{\bar{\mathbf{G}}}_t\left(k_\rho,k_\phi,z=h\,|\,z'=h;\omega\right)&\approx\tilde{\bar{\mathbf{G}}}_t^{\,\mathrm{int}}\left(k_\rho,k_\phi,z=h\,|\,z'=h;\omega\right)\\&=k_\rho\sum_{j=1}^{N_p}\tilde{\bar{\mathbf{A}}}_j(k_\phi,\omega)\cdot T_{j-1}\left(\frac{2k_\rho^{\mathrm{th}}}{k_\rho}-1\right).\end{aligned} \tag{10}$$

In (10), $T_{j-1}(\bullet)$ $(j=1,\ldots,N_p)$ stand for Chebyshev polynomials of the first kind, and the unknown matrices $\tilde{\bar{\mathbf{A}}}_j(k_\phi,\omega)$ $(j=1,\ldots,N_p)$ must be obtained for every pair of fixed values of k_ϕ and ω by making the matrix functions $\tilde{\bar{\mathbf{G}}}_t(k_\rho,k_\phi,z=h\,|\,z'=h;\omega)$ and $\tilde{\bar{\mathbf{G}}}_t^{\,\mathrm{int}}(k_\rho,k_\phi,z=h\,|\,z'=h;\omega)$ exactly coincide at the zeros of $T_{N_p}((2k_\rho^{\mathrm{th}})/(k_\rho)-1)$ in order to minimize interpolation errors (see [21] for more details). Numerical experiments have shown that the use of $N_p=3$ in (10) suffices to make $\tilde{\bar{\mathbf{G}}}_t$ and $\tilde{\bar{\mathbf{G}}}_t^{\,\mathrm{int}}$ coincide at least within six significant figures in the whole interval $k_\rho^{\mathrm{th}}<k_\rho<\infty$ when $|k_\phi-n\pi/2|>\pi/30(n=0,1,2,3,4)$. However, a value of N_p equal to five is necessary for reaching the same precision in the interpolation of $\tilde{\bar{\mathbf{G}}}_t$ via (10) when $|k_\phi-n\pi/2|\leq\pi/30(n=0,1,2,3,4)$ (in fact, it has been checked that, in this latter range of values of k_ϕ, the choice $N_p=3$ in (10) may lead to an inaccurate interpolation of $\tilde{\bar{\mathbf{G}}}_t$). Bearing in mind this fact, in this paper, the expression of (10) has always been used with a value of N_p equal to five as a way to ensure that the mentioned expression provides an accurate interpolation of $\tilde{\bar{\mathbf{G}}}_t$ in the whole interval $k_\rho^{\mathrm{th}}<k_\rho<\infty$ for any value of k_ϕ (note that this choice differs from that followed in [23], where a value of N_p equal to three was found to be enough in a similar interpolating expression). Once the matrix function $\tilde{\bar{\mathbf{G}}}_t^{\,\mathrm{int}}$ has been suitably chosen for providing an accurate approximation of $\tilde{\bar{\mathbf{G}}}_t$ in the interval $k_\rho^{\mathrm{th}}<k_\rho<\infty$ for any value of k_ϕ, this fact can be used for rewriting (10) as

$$\begin{aligned}\Gamma_{ij}(\omega)&=\frac{1}{4\pi^2}\int_0^{2\pi}\left\{\int_{0(C)}^{k_\rho^{\mathrm{th}}}\left[\left(\tilde{\mathbf{j}}_i^*(k_\rho,k_\phi)\right)^T\cdot\tilde{\bar{\mathbf{G}}}_t\left(k_\rho,k_\phi,z=h\,|\,z'=h;\omega\right)\cdot\tilde{\mathbf{j}}_j\left(k_\rho,k_\phi\right)\right]k_\rho\,dk_\rho\right.\\&\left.+\int_{k_\rho^{\mathrm{th}}}^{+\infty}\left[\left(\tilde{\mathbf{j}}_i^*(k_\rho,k_\phi)\right)^T\cdot\tilde{\bar{\mathbf{G}}}_t^{\,\mathrm{int}}\left(k_\rho,k_\phi,z=h\,|\,z'=h;\omega\right)\cdot\tilde{\mathbf{j}}_j\left(k_\rho,k_\phi\right)\right]k_\rho\,dk_\rho\right\}dk_\phi,\quad i,j=1,\ldots,N.\end{aligned} \tag{11}$$

The implementation of (11) is the final and crucial step of the technique for the fast computation of $\Gamma_{ij}(i,j=1,\ldots,N)$ in the spectral domain. It has been found that the finite integrals with respect to k_ϕ of (11) can be worked out to a high precision by means of a single 160-point Gauss–Legendre quadrature for-

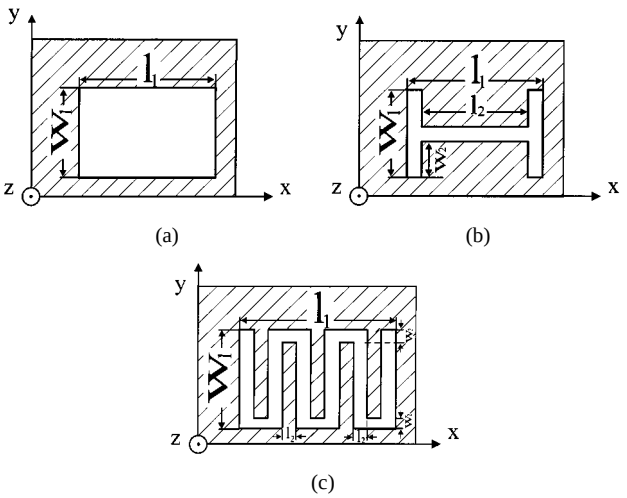

Fig. 2. Top views of microstrip patches of different shapes. (a) Rectangular shape. (b) H shape. (c) Meander shape. The coordinate axes coincide with those shown in Fig. 1.

mula, which means that the computation of each quantity Γ_{ij} reduces to the computation of 160 integrals with respect to k_ρ. In (11), each of these integrals with respect to k_ρ is split into a finite integral and one infinite integral. Whereas the finite integrals involve a relatively narrow interval and can be numerically carried out within short CPU times, the infinite integrals can be computed within even shorter CPU times for the particular choice of basis functions made in this paper by using the formulas supplied in the Appendix. As an estimate of the advantages of the use of (11), a comparison has been made between the total CPU time needed for the computation of $\det[\Gamma_{ij}(\omega)]$ (see (7)) when using (11) and that needed when using brute-force numerical integration via (9). Numerical experiments have shown that for the structures analyzed in Section III, the CPU times involved in the computation of $\det[\Gamma_{ij}(\omega)]$ by means of (11) are on average two orders of magnitude smaller than those obtained when using (9) when an accuracy of three significant figures in the value of $\det[\Gamma_{ij}(\omega)]$ is required.

III. Numerical Results

Fig. 2(a)–(c) shows the top views of the three types of microstrip patches with right-angle corners printed on ferrite substrates (rectangular-, H-, and meander-shaped patches) for which results are presented in this section. Additional results for microstrip patches with right-angle corners of any other shape can be easily generated by means of the numerical algorithm implemented by the authors.

In Table I(a) and (b), the convergence of the numerical method described in the previous section is checked with respect to the number of rooftop basis functions N used in the approximation of the current density. In particular, results are presented for the first five resonant modes of a rectangular microstrip patch printed on both a normally biased ferrite substrate and an in-plane biased ferrite substrate. Note that whereas the differences between the results obtained for the resonant frequencies when $N = 24$ and those obtained when $N = 264$ are within 5%, the differences between the results obtained for the resonant frequencies when $N = 112$ and those obtained when $N = 264$ are always within 0.8%. This seems to indicate that roughly 100 rooftop basis functions should suffice to provide reliable results for the resonant frequencies of the first resonant modes of a microstrip patch on a ferrite substrate. Table I(a) and (b) also shows that, for a given value of N, the higher the order of a resonant mode, the worse the accuracy of the result obtained for the resonant frequency, which is attributed to the fact that the current densities of the resonant modes become more oscillating and difficult to approximate as the order of the modes increases. Concerning the quality factors, they are obtained with less accuracy than the resonant frequencies because the imaginary parts of the results obtained for the complex resonant frequencies in Table I(a) and (b) are usually two or three orders of magnitude smaller than the real parts and, therefore, these imaginary parts are computed with less precision than the real parts. In particular, the discrepancies between the results derived from Table I(a) and (b) for the quality factors when $N = 112$ and those derived when $N = 264$ lie within 4%.

TABLE I
Convergence Pattern of the Complex Resonant Frequencies of the First Five Resonant Modes of a Rectangular Patch on (a) Normally and (b) in-Plane Biased Ferrite Substrates With Respect to the Number of Basis Functions Used in the Approximation of the Current Density ($w_1 = 4$ mm, $l_1 = 5.5$ mm, $h = 0.6$ mm, $\epsilon_f = 12.8, \mu_0 H_0 = 0.036$ T, $\mu_0 M_s = 0.178$ T, $\mu_0 \Delta H = 0$ T). The Modes Are Named After the Notation Used in the Cavity Model

$\theta_0 = \phi_0 = 0°$

Mode	$\omega_{mn}/2\pi$(GHz)		
(m,n)	$N = 24$	$N = 112$	$N = 264$
(1,0)	7.466+j0.043	7.352+j0.042	7.312+j0.042
(0,1)	11.73+j0.053	11.58+j0.051	11.53+j0.051
(1,1)	13.17+j0.021	12.88+j0.021	12.81+j0.021
(2,0)	16.63+j0.046	16.00+j0.039	15.90+j0.038
(0,2)	19.51+j0.017	18.71+j0.018	18.57+j0.018

(a)

$\theta_0 = 90°; \phi_0 = 0°$

Mode	$\omega_{mn}/2\pi$(GHz)		
(m,n)	$N = 24$	$N = 112$	$N = 264$
(1,0)	9.358+j0.020	9.265+j0.019	9.236+j0.019
(0,1)	10.01+j0.068	9.844+j0.066	9.790+j0.065
(1,1)	13.63+j0.029	13.43+j0.022	13.37+j0.021
(2,0)	16.35+j0.044	15.65+j0.036	15.53+j0.035
(0,2)	19.89+j0.054	19.12+j0.043	18.99+j0.041

(b)

TABLE II
RESONANT FREQUENCIES AND QUALITY FACTORS OF THE FIRST FIVE RESONANT MODES OF A RECTANGULAR PATCH ON (a) NORMALLY AND (b) IN-PLANE BIASED FERRITE SUBSTRATES ($w_1 = 4$ mm, $l_1 = 5.5$ mm, $h = 0.6$ mm, $\epsilon_f = 12.8, \mu_0 H_0 = 0.036$ T, $\mu_0 M_s = 0.178$ T, $\mu_0 \Delta H = 0$ T). THE MODES ARE NAMED AFTER THE NOTATION USED IN THE CAVITY MODEL. OUR RESULTS FOR THE RESONANT FREQUENCIES ARE COMPARED WITH THE NUMERICAL RESULTS OBTAINED IN [25] FOR THE *RCS* RESONANT PEAKS OF THE PATCH

$\theta_0 = \phi_0 = 0°$

Mode	Yang et al.[25] f_r^{mn}	This paper f_r^{mn}	This paper Q_{mn}
m=1,n=0	7.36	7.31	87.1
m=0,n=1	11.6	11.5	114
m=1,n=1	12.9	12.8	312
m=2,n=0	15.8	15.9	209
m=0,n=2	18.5	18.6	519

(a)

$\theta_0 = 90°; \phi_0 = 0°$

Mode	Yang et al.[25] f_r^{mn}	This paper f_r^{mn}	This paper Q_{mn}
m=1,n=0	9.22	9.24	241
m=0,n=1	9.75	9.79	75.2
m=1,n=1	13.6	13.4	326
m=2,n=0	15.4	15.5	222
m=0,n=2	19.0	19.0	232

(b)

In Table II(a) and (b), the authors test the validity of the numerical method described in Section II by comparing their numerical results for the resonant frequencies of the microstrip patch analyzed in Table I(a) and (b) [$N = 264$ has been used in Table II(a) and (b)] with numerical results published in [25] for the *RCS* resonant peaks of the same patch. It can be verified that the differences between the two sets of results for the resonant frequencies are always within 1.5%. Table II(a) and (b) also shows the numerical results obtained for the quality factors of the resonant modes analyzed.

In Fig. 3, results are presented for the resonant frequencies of the first three resonant modes of a rectangular microstrip patch printed on a normally biased ferrite as a function of the magnitude of the bias magnetic field. This figure is analogous to that presented in [17] for the resonant frequencies of the first five resonant modes of a circular microstrip patch on a normally biased ferrite. As in [17], in Fig. 3, there is a cutoff frequency region $f_1 = \omega_0/2\pi < f < f_2 = \sqrt{\omega_0(\omega_0 + \omega_m)}/2\pi$ ($\omega_0 = \gamma\mu_0 H_0$ and $\omega_m = \gamma\mu_0 M_s$) in which resonances cannot occur because of the excitation in that frequency region of an infinite number of forward magnetostatic volume-wave (FMSVW) modes along the ferrite substrate in all the directions of the plane X-Y of Fig. 2(a) [26]. Also, the resonant frequencies of all resonant modes appear above and below the cutoff frequency region as it happens in [17]. Fig. 3 shows that the resonant frequencies of the three resonant modes analyzed can be tuned over a wide frequency range by means of the bias magnetic field as predicted in [6]. In particular, the resonant frequency of the fundamental mode ($m = 1, n = 0$) changes more than 50% when $\mu_0 H_0$ is varied from 0 to 0.4 T both below the cutoff frequency region and above that frequency region.

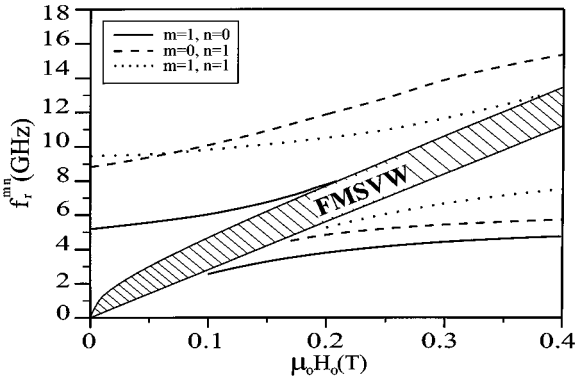

Fig. 3. Resonant frequencies of the first three resonant modes of a rectangular microstrip patch on a normally biased ferrite substrate ($w_1 = 5$ mm, $l_1 = 6.5$ mm, $h = 1.27$ mm, $\epsilon_f = 15, \mu_0 M_s = 0.178$ T, $\mu_0 \Delta H = 0.001$ T, $\theta_0 = \phi_0 = 0°$). The modes are named after the notation used in the cavity model. The striped frequency band stands for the propagation region of FMSVW modes.

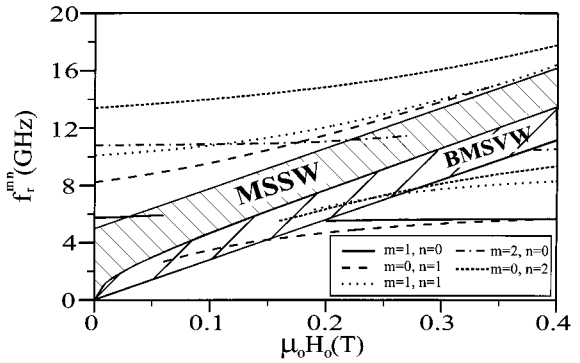

Fig. 4. Resonant frequencies of the first five resonant modes of a rectangular microstrip patch on an in-plane biased ferrite substrate ($w_1 = 5$ mm, $l_1 = 6.5$ mm, $h = 1.27$ mm, $\epsilon_f = 15, \mu_0 M_s = 0.178$ T, $\mu_0 \Delta H = 0.001$ T, $\theta_0 = \phi_0 = 90°$). The modes are named after the notation used in the cavity model. The striped frequency bands stand for the propagation regions of BMSVW and MSSW modes.

In Fig. 4, the authors plot the resonant frequencies of the first five resonant modes of a rectangular microstrip patch printed on an in-plane biased ferrite versus the magnitude of the bias magnetic field. Note that, in this case, some results for the resonant frequencies have been obtained within the propagation regions of magnetostatic modes. Since the propagation of magnetostatic modes involves the appearance of unbounded poles in the spectral Green's function $\tilde{\mathbf{G}}_t(k_\rho, k_\phi, z = h \,|\, z' = h; \omega)$

of (9), ferrite losses have been included ($\Delta H \neq 0$) so as to keep these poles below the integration path C of (9) for every value of k_ϕ [9]. It can be noticed that whereas the resonant frequencies of the modes $m = 0, n = 1, m = 0, n = 2$ and $m = 1, n = 1$ analyzed in Fig. 4 can be tuned by means of the bias magnetic field, as it happens in Fig. 3, the other two resonant modes $m = 1, n = 0$ and $m = 2, n = 0$ are practically unaffected by the variations in the magnitude of the bias magnetic field. The explanation for this latter behavior is that the interaction between the dc-bias magnetic field and the ac magnetic field existing around the patch of Fig. 4 is very weak in the resonant modes $m = 1, n = 0$ and $m = 2, n = 0$ because the ac magnetic field of these two modes is mainly parallel to the dc magnetic field [directed along the Y axis of Fig. 2(a)] [27]. However, this does not happen in the case of the modes $m = 0, n = 1, m = 0, n = 2$ and $m = 1, n = 1$ analyzed in Fig. 4 and in the case of the modes analyzed in Fig. 3. In fact, maximum interaction between the dc and ac magnetic fields is expected for the modes $m = 0, n = 1$ and $m = 0, n = 2$ of Fig. 4 and the modes of Fig. 3 because the ac magnetic field of all these modes is mainly perpendicular to the dc-bias magnetic field [27]. Fig. 4 also shows that the resonant frequencies of the resonant modes $m = 0, n = 1$ and $m = 0, n = 2$ occupy part of the region of propagation of backward magnetostatic volume-wave (BMSVW) modes $f_1 < f < f_2$, but do not occupy the region of propagation of magnetostatic surface wave (MSSW) modes $f_2 < f < f_3 = (\omega_0 + \omega_m)/2\pi$ [26]. This is because the currents of these two resonant modes are mainly directed along the Y axis of Fig. 2(a)—which is the direction of the bias magnetic field—and, therefore, these modes may excite MSSW modes propagating in a direction perpendicular to that of the currents (as it happens with the MSSW transducers described in [28] and [29]), but cannot excite BMSVW modes propagating in the direction of the currents. The opposite holds for the resonant modes $m = 1, n = 0$ and $m = 2, n = 0$ whose resonant frequencies occupy the region of propagation of MSSW modes, but do not occupy the region of propagation of BMSVW modes. In this latter case, the currents of the two resonant modes are mainly directed along the X axis of Fig. 2(a) (i.e., perpendicular to the direction of the bias magnetic field) and, therefore, the resonant modes may excite BMSVW modes propagating in a direction perpendicular to that of the currents (as it happens with the magnetostatic backward volume wave transducer described in [30]), but cannot excite MSSW modes propagating in the direction of the currents. Finally, the current of the resonant mode $m = 1, n = 1$ has both X- and Y-components and, therefore, this resonant mode may excite magnetostatic modes propagating in a direction making an angle between 0° and 90° with the direction of the bias magnetic field. These magnetostatic modes may be BMSVW and/or MSSW modes depending on the direction of propagation and the magnitude of the bias magnetic field [26], which justifies that the resonant frequencies of the mode $m = 1, n = 1$ may occupy the region of propagation of BMSVW modes and/or the region of propagation of MSSW modes.

In Fig. 5, our numerical results for the resonant frequencies of some of the resonant modes of a square microstrip patch on an in-plane biased ferrite are compared with measurements published in [18] with a view to validating the generic behavior of part of the results plotted in Fig. 4. The agreement between numerical and experimental results in Fig. 5 is good. The differences are on average within 2% for the modes $m = 0, n = 1$ and $m = 0, n = 2$, and within 4% for the mode $m = 0, n = 3$. Note that the experimental resonant frequencies of the three resonant modes analyzed in Fig. 5 occupy the region of propagation of BMSVW modes, but do not occupy the region of propagation of MSSW modes, which is coherent with the theoretical prediction provided by the numerical results of Fig. 4. Also, note that the experimental resonant frequencies of the three resonant modes appear above and below the region of propagation of MSSW modes, which is again in agreement with the behavior appearing in Fig. 4. It should be pointed out that, although the resonant frequencies of other resonant modes ($m = 1, n = 0, m = 1, n = 1, m = 2, n = 0$) were numerically found in between the resonant frequencies plotted in Fig. 5, these other resonant frequencies were not experimentally detected in [18], which is attributed to the type of excitation mechanism used in the measurements of this latter paper.

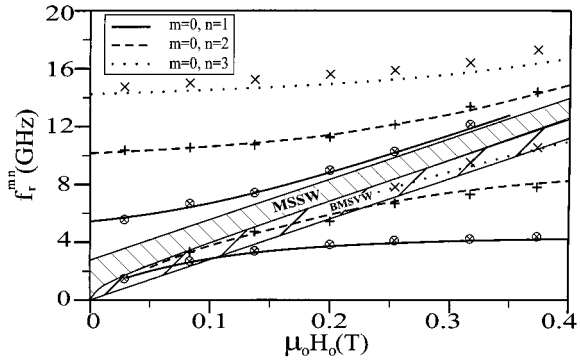

Fig. 5. Resonant frequencies of three of the resonant modes of a square microstrip patch on an in-plane biased ferrite substrate ($w_1 = l_1 = 9.525$ mm, $h = 0.508$ mm, $\epsilon_f = 11.41, \mu_0 M_s = 0.0985$ T, $\mu_0 \Delta H = 0.001$ T, $\theta_0 = \phi_0 = 90°$). The modes are named after the notation used in the cavity model. The striped frequency bands stand for the propagation regions of BMSVW and MSSW modes. Our results (solid, dashed, and dotted lines) are compared with those obtained in [18] ($\times$, $+$ and $\otimes$).

In Fig. 6, results are presented for the resonant frequencies of the first three resonant modes of a rectangular microstrip patch printed on a ferrite substrate with bias magnetic field oriented in a direction which makes an angle of 45° with the normal to the substrate. It can be recognized that among the three resonant modes, the mode $m = 0, n = 1$ is the most sensible to variations in the magnitude of the bias magnetic field since this is the only mode for which the ac magnetic field is mainly perpendicular to the dc magnetic field. For the orientation of the bias magnetic field considered in Fig. 6, the ferrite substrate supports the propagation of BMSVW modes in the frequency region $f_1 < f < f_4 = \sqrt{\omega_0(\omega_0 + \omega_m/2)}/2\pi$, the propagation of FMSVW modes in the frequency region $f_4 < f < f_2$, and the propagation of MSSW modes in the frequency region $f_2 < f < f_5$ (where $f_5 < f_3$). Note that the resonant frequencies of the three resonant modes analyzed in Fig. 6 occupy part of the regions of propagation of BMSVW modes and MSSW modes, just as it happens in Fig. 4. However, resonances never occur in the region of propagation of FMSVW modes, which is in agreement with the results obtained in Fig. 3.

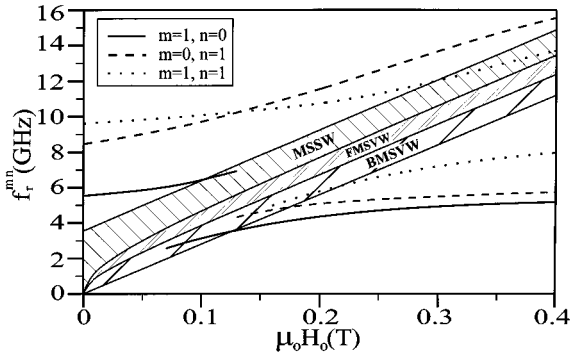

Fig. 6. Resonant frequencies of the first three resonant modes of a rectangular microstrip patch on a ferrite substrate with inclined bias magnetic field ($w_1 = 5$ mm, $l_1 = 6.5$ mm, $h = 1.27$ mm, $\epsilon_f = 15, \mu_0 M_s = 0.178$ T, $\mu_0 \Delta H = 0.001$ T, $\theta_0 = 45°, \phi_0 = 90°$). The modes are named after the notation used in the cavity model. The striped frequency bands stand for the propagation regions BMSVW, FMSVW, and MSSW modes.

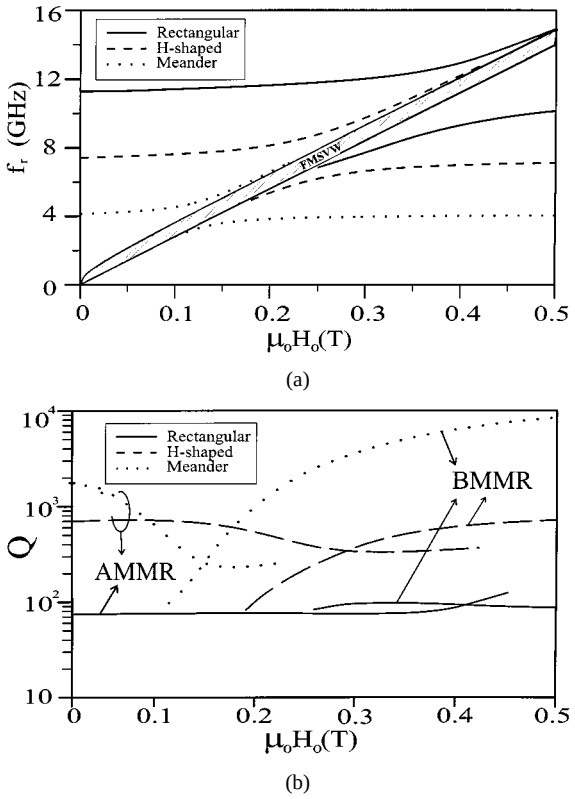

Fig. 7. (a) Resonant frequencies and (b) quality factors of the fundamental resonant mode of three microstrip patches (rectangular, H-, and meander shaped) on a normally biased ferrite substrate ($w_1 = 2.5$ mm, $l_1 = 3.25$ mm, $h = 0.635$ mm; ferrite substrate: $\epsilon_f = 15, \mu_0 M_s = 0.068$ T, $\mu_0 \Delta H = 0.001$ T, $\theta_0 = \phi_0 = 0°$; H-shaped patch: $l_2 = (9/11)l_1$, $w_2 = (4/9)w_1$; meander-shaped patch: $l_2 = (1/11)l_1, w_2 = (1/9)w_1$). In Fig. 7(a), the striped frequency band stands for the propagation region of FMSVW modes and, in Fig. 7(b), AMMR stands for resonances above the region of FMSVW modes and BMMR stands for resonances below the region of FMSVW modes.

In Fig. 7(a) and (b), results are plotted for the resonant frequencies and quality factors of the fundamental resonant mode of rectangular microstrip, an H-shaped, and a meander-shaped patches. The patches are assumed to be fabricated on the same normally biased ferrite substrate occupying the same overall

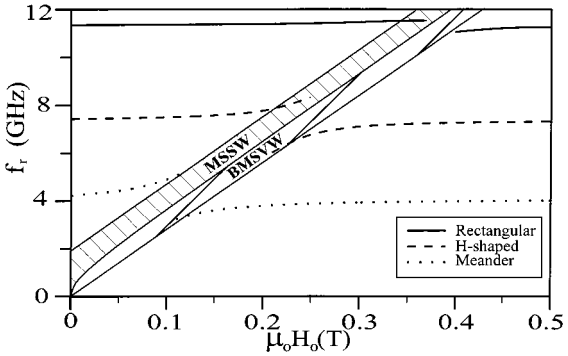

Fig. 8. Resonant frequencies of the fundamental resonant mode of three microstrip patches (rectangular, H-, and meander shaped) on an in-plane biased ferrite substrate ($w_1 = 2.5$ mm, $l_1 = 3.25$ mm, $h = 0.635$ mm; ferrite substrate: $\epsilon_f = 15, \mu_0 M_s = 0.068$ T, $\mu_0 \Delta H = 0.001$ T, $\theta_0 = \phi_0 = 90°$; H-shaped patch: $l_2 = (9/11)l_1, w_2 = (4/9)w_1$; meander-shaped patch: $l_2 = (1/11)l_1, w_2 = (1/9)w_1$). The striped frequency bands stand for the propagation regions of BMSVW and MSSW modes.

substrate size (given by $l_1 \times w_1$). Note that the resonant frequencies of the meander-shaped patch are always smaller than those of the H-shaped and rectangular patches, which indicates that the meander-shaped patch shows the best performance for size-reduction applications. However, the quality factors of the meander-shaped patch are usually larger than those of the H-shaped patch and the rectangular patch and, therefore, the bandwidths of the meander-shaped patch are usually smaller than those of the H-shaped and rectangular patches, which is a clear disadvantage when the patches are used as antennas. Fig. 7(a) shows that the resonant frequencies of the three patches analyzed can be tuned over a wide frequency range by varying the magnitude of the bias magnetic field. The meander- and the H-shaped patches turn out to be more tunable than the rectangular patch above the region of propagation of FMSVW modes (in fact, the resonant frequency of the fundamental resonant mode of the meander- and H-shaped patches changes more than 70% when $\mu_0 H_0$ is varied from 0 to 0.5 T), but the rectangular patch is more tunable than the other two patches below the region of propagation of FMSVW modes (in this latter case, the resonant frequency of the fundamental resonant mode of the rectangular patch changes roughly 50% when $\mu_0 H_0$ is varied from 0 to 0.5 T).

In Figs. 8 and 9, the authors plot the resonant frequencies of the fundamental resonant mode of the three patches analyzed in Fig. 7(a) and (b) in the cases in which the ferrite substrate is in-plane biased along the X and Y axes shown in Figs. 2(a)–(c). In Fig. 8, the ferrite substrate is biased along the Y axis and, in this figure, the fundamental resonant mode of the meander-shaped patch is more affected by variations in the magnitude of the bias magnetic field than the resonant modes of the H-shaped and rectangular patches. The explanation for this behavior is that, whereas the current of the resonant mode of the meander-shaped patch is mainly directed along the Y axis, the currents of both the H-shaped and the rectangular patches are mainly directed along the X axis and, therefore, whereas the ac magnetic field of the resonant mode of the meander-shaped patch is mainly perpendicular to the dc-bias magnetic field, the ac magnetic fields of the resonant modes of the H-shaped and rectangular patches are mainly parallel to the dc magnetic field.

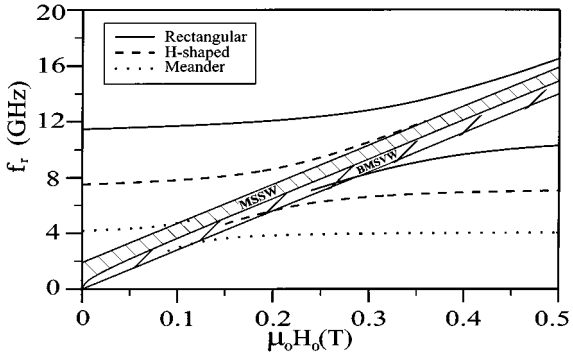

Fig. 9. Resonant frequencies of the fundamental resonant mode of three microstrip patches (rectangular, H-, and meander shaped) on an in-plane biased ferrite substrate ($w_1 = 2.5$ mm, $l_1 = 3.25$ mm, $h = 0.635$ mm; ferrite substrate: $\epsilon_f = 15, \mu_0 M_s = 0.068$ T, $\mu_0 \Delta H = 0.001$ T, $\theta_0 = 90°$, $\phi_0 = 0°$; H-shaped patch: $l_2 = (9/11)l_1, w_2 = (4/9)w_1$; meander-shaped patch: $l_2 = (1/11)l_1, w_2 = (1/9)w_1$). The striped frequency bands stand for the propagation regions of BMSVW and MSSW modes.

The opposite holds for Fig. 9. In this figure, the ferrite substrate is biased along the X axis and, in this case, whereas the ac magnetic field of the meander-shaped patch is mainly parallel to the dc magnetic field, the ac magnetic field of the H-shaped and rectangular patches are mainly perpendicular to the dc magnetic field, which justifies that the resonant modes of the H-shaped and rectangular patches are much more tunable by the magnitude of the bias magnetic field than the resonant mode of the meander-shaped patch. As shown in the comments of Fig. 4, the penetration of the resonant frequencies of the three resonant modes analyzed in Figs. 8 and 9 inside the regions of propagation of magnetostatic modes can be explained in terms of the direction of the currents of those three resonant modes. In fact, whereas in Fig. 8 the resonant frequencies of the meander-shaped patch mainly occupy the region of propagation of BMSVW modes (which cannot be excited by currents parallel to the bias magnetic field) and the resonant frequencies of the H-shaped and rectangular patches mainly occupy the region of propagation of MSSW modes (which cannot be excited by currents perpendicular to the bias magnetic field), in Fig. 9, the resonant frequencies of the meander-shaped patch mainly occupy the region of propagation of MSSW modes, and the resonant frequencies of the H-shaped and rectangular patches mainly occupy the region of propagation of BMSVW modes.

IV. Conclusion

Galerkin's method in the spectral domain has been used for the determination of the resonant frequencies and quality factors of the resonant modes of microstrip patches with right-angle corners of arbitrary shape in the case in which the substrate of the patches is a magnetized ferrite with arbitrarily oriented bias magnetic field. A special technique has been developed for accelerating the numerical computation of the double infinite integrals arising from the application of Galerkin's method in the spectral domain. The results obtained show that the resonant frequencies of a microstrip patch printed on a ferrite substrate can always be tuned by varying the magnitude of the bias magnetic field. Maximum tunability is achieved when the dc-bias magnetic field is mainly perpendicular to the ac magnetic field existing around the resonant patch, and minimum tunability results when the dc magnetic field is mainly parallel to the ac magnetic field. The authors have found that resonances are not possible inside the frequency region of propagation of FMSVW modes along the ferrite substrate. However, resonances may occur inside the frequency regions of propagation of BMSVW modes and MSSW modes provided these magnetostatic modes are not excited by the currents of the resonant modes of the patch. Finally, the meander- and the H-shaped patches have proven to have size reduction capabilities with respect to the rectangular patch at the expense of showing smaller bandwidth.

Appendix

When subsectional rooftop basis functions are used in (4) for approximating the current density on the microstrip patch of Fig. 1(a) and a value of N_p equal to five is used in (10) in the interpolating expression of the asymptotic spectral dyadic Green's function, after some cumbersome manipulations, it can be shown that the infinite integrals with respect to k_ρ appearing in (11) can all be expressed as linear combinations of integrals of the type

$$I_S(\gamma, k) = \int_\gamma^\infty \frac{\sin x}{x^k}\, dx, \qquad 4 \le k \le 8; \gamma > 0 \quad (12)$$

$$I_C(\gamma, k) = \int_\gamma^\infty \frac{\cos x}{x^k}\, dx, \qquad 4 \le k \le 8; \gamma > 0 \quad (13)$$

where the values of the variable γ, which are required for the evaluation of every infinite integral of (11), are strongly dependent on the values of i, j and k_ϕ involved in that integral.

In principle, the integrals of (12) and (13) can be obtained by means of the forward recurrence expressions [23]

$$I_S(\gamma, k) = \left(\frac{1}{k-1}\right)\frac{\sin\gamma}{\gamma^{k-1}} + \left(\frac{1}{k-1}\right) I_C(\gamma, k-1), \quad k \ge 2 \quad (14)$$

$$I_C(\gamma, k) = \left(\frac{1}{k-1}\right)\frac{\cos\gamma}{\gamma^{k-1}} - \left(\frac{1}{k-1}\right) I_S(\gamma, k-1), \quad k \ge 2 \quad (15)$$

which are initialized by means of the equations

$$I_S(\gamma, k=1) = \frac{\pi}{2} - \mathrm{Si}(\gamma) \quad (16)$$

$$I_C(\gamma, k=1) = -\mathrm{Ci}(\gamma) \quad (17)$$

where $\mathrm{Si}(\bullet)$ and $\mathrm{Ci}(\bullet)$ are sine and cosine integrals, which can be obtained with reasonable accuracy by means of the subroutine "CISIA" published in [31].

The problem arising from the recurrence expressions of (14) and (15) is that they are unstable and lose accuracy as k increases. Also, the subroutine CISIA used for the calculation of $\mathrm{Si}(\gamma)$ and $\mathrm{Ci}(\gamma)$ has been found to lose some accuracy as γ increases. As a consequence of the combined effect of these two latter facts, numerical experiments have shown that (14)–(17) turn out to be slightly inaccurate for the calculation of the ten integrals of (12) and (13) when $\gamma > 10$ (the larger the value of k, the larger the inaccuracies). Also, the authors have found that these inaccuracies may be critical when the results provided

by (14)–(17) are used in the calculation of the infinite integrals of (11) in those cases in which $|k_\phi - n\pi/2| \leq \pi/30 (n = 0, 1, 2, 3, 4)$. Therefore, the expressions (14)–(17) should not be used for the computation of the infinite integrals of (11) when $\gamma > 10$. The following expressions should be used instead:

$$I_S(\gamma, k) = \mathrm{Im}\left[j e^{j\gamma} \int_0^\infty \frac{e^{-t}}{(\gamma + jt)^k}\, dt \right] \tag{18}$$

$$I_C(\gamma, k) = \mathrm{Re}\left[j e^{j\gamma} \int_0^\infty \frac{e^{-t}}{(\gamma + jt)^k}\, dt \right]. \tag{19}$$

Equations (18) and (19) have been obtained by means of the Cauchy–Riemann residue theorem. Numerical experiments have shown that the infinite integrals of (18) and (19) can be computed by means of a ten-point Gauss–Laguerre quadrature with high accuracy independently of the value of k, which indicates that (18) and (19) basically lead to accurate closed-form expressions for the computation of (12) and (13) when $\gamma > 10$.

Although the technique for the computation of (12) and (13) based on the use of (18) and (19) is reliable when $\gamma > 10$, the authors have found an alternative technique for the computation of (12) and (13), which is even more accurate and faster than the former technique when $\gamma > 25$. This alternative technique is based on the backward recurrence expressions

$$I_S(\gamma, k) = \frac{\cos\gamma}{\gamma^k} - k I_C(\gamma, k+1), \qquad k \geq 1 \tag{20}$$

$$I_C(\gamma, k) = -\frac{\sin\gamma}{\gamma^k} + k I_S(\gamma, k+1), \qquad k \geq 1. \tag{21}$$

These recurrence expressions are initialized by the truncated asymptotic expansions of $I_S(\gamma, k)$ and $I_C(\gamma, k)$ for $\gamma \gg$ when $k = k_{\max} \gg$, which are given by

$$I_S(\gamma, k = k_{\max}) \approx \frac{\cos\gamma}{\gamma^{k_{\max}}} f_1(\gamma, k = k_{\max}) + \frac{\sin\gamma}{\gamma^{(k_{\max}+1)}} f_2(\gamma, k = k_{\max}) \tag{22}$$

$$I_C(\gamma, k = k_{\max}) \approx -\frac{\sin\gamma}{\gamma^{k_{\max}}} f_1(\gamma, k = k_{\max}) + \frac{\cos\gamma}{\gamma^{(k_{\max}+1)}} f_2(\gamma, k = k_{\max}) \tag{23}$$

where

$$f_1(\gamma, k) = 1 - \frac{k(k+1)}{\gamma^2} \tag{24}$$

$$f_2(\gamma, k) = k - \frac{k(k+1)(k+2)}{\gamma^2}. \tag{25}$$

As stated above, the use of (20)–(25) with $k_{\max} = 20$ has been found to provide a technique for the computation of (12) and (13), which is preferred to (18) and (19) when $\gamma > 25$.

To sum up, we should say that the most suitable technique for the computation of the ten integrals of (12) and (13) is that based on (14)–(17) in the interval $0 < \gamma \leq 10$, that based on the expressions (18) and (19) in the interval $10 < \gamma \leq 25$, and finally, that based on (20)–(25) (with $k_{\max} = 20$) in the interval $25 < \gamma < \infty$.

REFERENCES

[1] V. Palanisamy and R. Garg, "Rectangular ring and H-shaped microstrip antennas-alternatives to rectangular patch antenna," *Electron. Lett.*, vol. 21, no. 19, pp. 874–876, 1985.

[2] H. Y. Wang and M. J. Lancaster, "Aperture-coupled thin-film superconducting meander line antennas," *IEEE Trans. Antennas Propagat.*, vol. 47, pp. 829–836, May 1999.

[3] K. Araki, D. I. Kim, and Y. Naito, "A study on circular disk resonators on a ferrite substrate," *IEEE Trans. Microwave Theory Tech.*, vol. MTT-30, pp. 147–154, Feb. 1982.

[4] M. Tsutsumi and T. Fukusako, "Broadband magnetically tunable superconducting microstrip resonator using yttrium iron garnet single crystal," *Electron. Lett.*, vol. 33, no. 8, pp. 687–688, 1997.

[5] T. Fukusako and M. Tsutsumi, "Superconducting microstrip resonator with yttrium iron garnet single crystal," *IEEE Trans. Microwave Theory Tech.*, vol. 45, pp. 2013–2017, Nov. 1997.

[6] D. M. Pozar and V. Sanchez, "Magnetic tuning of a microstrip antenna on a ferrite substrate," *Electron. Lett.*, vol. 24, no. 12, pp. 729–731, 1988.

[7] H. Y. Yang, J. A. Castaneda, and N. G. Alexopoulos, "Multifunctional and low *RCS* nonreciprocal microstrip antennas," *Electromagnetics*, vol. 12, pp. 17–31, 1992.

[8] D. M. Pozar and H. Y. Yang, "Corrections to 'Radiation and scattering characteristics of microstrip antennas on normally biased ferrite substrates'," *IEEE Trans. Antennas Propagat.*, vol. 42, pp. 122–123, Jan. 1994.

[9] H. Y. Yang, "Characteristics of switchable ferrite microstrip antennas," *IEEE Trans. Antennas Propagat.*, vol. 44, pp. 1127–1132, Aug. 1996.

[10] J. S. Roy, P. Vaudon, A. Reineix, F. Jecko, and B. Jecko, "Circularly polarized far fields of an axially magnetized circular ferrite microstrip antenna," *Microwave Opt. Technol. Lett.*, vol. 5, no. 5, pp. 228–230, May 1992.

[11] D. M. Pozar, "Radiation and scattering characteristics of microstrip antennas on normally biased ferrite substrates," *IEEE Trans. Antennas Propagat.*, vol. 40, pp. 1084–1092, Sept. 1992.

[12] P. J. Rainville and F. J. Harackiewicz, "Magnetic tuning of a microstrip patch antenna fabricated on a ferrite film," *IEEE Microwave Guided Wave Lett.*, vol. 2, pp. 483–485, Dec. 1992.

[13] N. E. Buris, T. B. Funk, and R. S. Silverstein, "Dipole arrays printed on ferrite substrates," *IEEE Trans. Antennas Propagat.*, vol. 41, pp. 165–175, Feb. 1993.

[14] S. Nam and T. Itoh, "Calculation of accurate complex resonant frequency of an open microstrip resonator using the spectral domain method," *J. Electromagn. Waves Applicat.*, vol. 2, no. 7, pp. 635–651, 1988.

[15] W. C. Chew and Q. Liu, "Resonance frequency of a rectangular microstrip patch," *IEEE Trans. Antennas Propagat.*, vol. 36, pp. 1045–1056, Aug. 1988.

[16] Z. Cai and J. Bornemann, "Rigorous analysis of radiation properties of lossy patch resonators on complex anisotropic media and lossy ground metallization," *IEEE Trans. Antennas Propagat.*, vol. 42, pp. 1443–1446, Oct. 1994.

[17] V. Losada, R. R. Boix, and M. Horno, "Full-wave analysis of circular microstrip resonators in multilayered media containing uniaxial anisotropic dielectrics, magnetized ferrites and chiral materials," *IEEE Trans. Microwave Theory Tech.*, vol. 48, pp. 1057–1064, June 2000.

[18] H. How, T. M. Fang, and C. Vittoria, "Intrinsic modes of radiation in ferrite patch antennas," *IEEE Trans. Microwave Theory Tech.*, vol. 42, pp. 988–994, June 1994.

[19] H. Y. Yang, J. A. Castaneda, and N. G. Alexopoulos, "Surface wave modes of printed circuits on ferrite substrates," *IEEE Trans. Microwave Theory Tech.*, vol. 40, pp. 613–621, Apr. 1992.

[20] D. M. Pozar, *Microwave Engineering*. Reading, MA: Addison-Wesley, 1990.

[21] R. R. Boix, N. G. Alexopoulos, and M. Horno, "Efficient numerical computation of the spectral transverse dyadic Green's function in stratified anisotropic media," *J. Electromagn. Waves Applicat.*, vol. 10, no. 8, pp. 1047–1083, 1996.

[22] A. W. Glisson and D. R. Wilton, "Simple and efficient numerical methods for problems of electromagnetic radiation and scattering from sources," *IEEE Trans. Antennas Propagat.*, vol. AP-28, pp. 593–603, Sept. 1980.

[23] V. Losada, R. R. Boix, and M. Horno, "Resonant modes of circular microstrip patches in multilayered substrates," *IEEE Trans. Microwave Theory Tech.*, vol. 47, pp. 488–498, Apr. 1999.

[24] H. Y. Yang and N. G. Alexopoulos, "Basic blocks for high frequency interconnects: Theory and experiment," *IEEE Trans. Microwave Theory Tech.*, vol. 36, pp. 1258–1264, Aug. 1988.
[25] H. Y. Yang, J. A. Castaneda, and N. G. Alexopoulos, "The *RCS* of a microstrip patch on an arbitrarily biased ferrite substrate," *IEEE Trans. Antennas Propagat.*, vol. 41, pp. 1610–1614, Dec. 1993.
[26] M. S. Sodha and N. C. Srivastava, *Microwave Propagation in Ferrimagnetics*. New York, NY: Plenum, 1981.
[27] R. Marques, "Ferrite loaded waveguides," in *Wiley Encyclopaedia of Electrical and Electronics Engineering*. New York: Wiley, 1999, vol. 7, pp. 355–364.
[28] A. K. Ganguly and D. C. Webb, "Microstrip excitation of magnetostatic surface waves: Theory and experiment," *IEEE Trans. Microwave Theory Tech.*, vol. MTT-23, pp. 998–1006, Dec. 1975.
[29] E. B. El-Sharawy and R. W. Jackson, "Full-wave analysis of an infinitely long magnetic surface wave transducer," *IEEE Trans. Microwave Theory Tech.*, vol. 38, pp. 730–737, June 1990.
[30] J. P. Parekh and M. S. Tuan, "Excitation of magnetostatic backward volume waves," *IEEE Trans. Magn.*, vol. MAG-16, pp. 1165–1167, Sept. 1980.
[31] S. Zhang and J. Jin, *Computation of Special Functions*. New York: Wiley, 1996.

Germán León was born in Alcázar de San Juan, Spain, in 1975. He received the Licenciado degree in physics from the University of Seville, Seville, Spain, in 1998, and is currently working toward the Ph.D. degree in electronics and electromagnetism at the University of Seville.

His research interests focus on the effect of ferrite substrates on the performance of planar passive microwave circuits and printed circuit antennas.

Mr. León was the recipient of a 1999 scholarship presented by the Spanish Ministry of Education and Culture.

Rafael R. Boix (M'96) was born in Melilla, Spain, in 1962. He received the Licenciado and Doctor degrees in physics from the University of Seville, Seville, Spain, in 1985 and 1990, respectively.

Since 1985, he has been with the Electronics and Electromagnetics Department, University of Seville, where he became an Associate Professor in 1994. During the summers of 1991 and 1992, he was a Visiting Scholar with the Electrical Engineering Department, University of California at Los Angeles (UCLA). During the summer of 1996, he was a Visiting Scholar with the Electrical and Computer Engineering Department, Syracuse University, Syracuse, NY. His current research interest are focused on the analysis of the effects of complex substrates on the performance of planar passive microwave circuits, planar periodic transmission lines, frequency-selective surfaces, and printed circuit antennas.

Dr. Boix is on the Editorial Board of the IEEE TRANSACTIONS ON MICROWAVE THEORY AND TECHNIQUES.

Francisco Medina (M'90–SM'01) was born in Puerto Real, Cádiz, Spain, in November 1960. He received the Licenciado and Doctor degrees from the University of Seville, Seville, Spain, in 1983 and 1987, respectively, both in physics.

From 1986 to 1987, he spent the academic year with the Laboratoire de Microondes de l'ENSEEIHT, Toulouse, France. From 1985 to 1989, he was a Profesor Ayudante (Assistant Professor) with the Departamento de Electrónica y Electromagnetismo, University of Seville, and since 1990, he has been a Profesor Titular (Associate Professor) of electromagnetism. He is also currently Head of the Microwaves Group, University of Seville. His research interest includes analytical and numerical methods for guidance, resonant and radiating structures, passive planar circuits, and the influence on these circuits of anisotropic materials.

Dr. Medina was a member of both the Technical Program Committee (TPC) of the 23rd European Microwave Conference, Madrid, Spain, 1993, and the TPC of ISRAMT'99, Malaga, Spain. He is on the Editorial Board of the IEEE TRANSACTIONS ON MICROWAVE THEORY AND TECHNIQUES. He has been a reviewer for other IEEE and Institution of Electrical Engineers (IEE), U.K., publications.